BBA - General Subjects 1862 (2018) 836–845

Contents lists available at ScienceDirect

BBA - General Subjects

journal homepage: www.elsevier.com/locate/bbagen

Water-mediated interactions enable smooth substrate transport in a bacterial efflux pump

Attilio Vittorio Vargiu[a,*], Venkata Krishnan Ramaswamy[a], Ivana Malvacio[a], Giuliano Malloci[a], Ulrich Kleinekathöfer[b], Paolo Ruggerone[a]

[a] Department of Physics, University of Cagliari, s.p. 8, Cittadella Universitaria, 09042 Monserrato (CA), Italy
[b] Department of Physics & Earth Sciences, Jacobs University Bremen, Campus Ring 1, 28759 Bremen, Germany

ARTICLE INFO

Keywords:
Multi-drug resistance
RND efflux pumps
AcrB
Molecular dynamics
Enhanced-sampling
Free energy calculations

ABSTRACT

Background: Efflux pumps of the Resistance-Nodulation-cell Division superfamily confer multi-drug resistance to Gram-negative bacteria. The most-studied polyspecific transporter belonging to this class is the inner-membrane trimeric antiporter AcrB of *Escherichia coli*. In previous studies, a functional rotation mechanism was proposed for its functioning, according to which the three monomers undergo concerted conformational changes facilitating the extrusion of substrates. However, the molecular determinants and the energetics of this mechanism still remain unknown, so its feasibility must be proven mechanistically.

Methods: A computational protocol able to mimic the functional rotation mechanism in AcrB was developed. By using multi-bias molecular dynamics simulations we characterized the translocation of the substrate doxorubicin driven by conformational changes of the protein. In addition, we estimated for the first time the free energy profile associated to this process.

Results: We provided a molecular view of the process in agreement with experimental data. Moreover, we showed that the conformational changes occurring in AcrB enable the formation of a layer of structured waters on the internal surface of the transport channel. This water layer, in turn, allows for a fairly constant hydration of the substrate, facilitating its diffusion over a smooth free energy profile.

Conclusions: Our findings reveal a new molecular mechanism of polyspecific transport whereby water contributes by screening potentially strong substrate-protein interactions.

General significance: We provided a mechanistic understanding of a fundamental process related to multi-drug transport. Our results can help rationalizing the behavior of other polyspecific transporters and designing compounds avoiding extrusion or inhibitors of efflux pumps.

1. Introduction

Multi-Drug Resistant (MDR) bacteria represent one of the most pressing health concerns of the XXI Century due to their ability to elude the action of most (if not all) antibiotics [1–4]. Efflux pumps are a special family of membrane transport proteins that shuttle a broad spectrum of chemically unrelated cytotoxic molecules out of bacteria, thus playing a major role in conferring the MDR phenotype [5–9]. Polyspecificity and partial overlap among the substrate specificities of different pumps are striking properties of these efflux machineries [10, 11], making them a key survival tool of bacteria.

The efflux systems of the Resistance Nodulation-cell Division (RND) superfamily, which span the entire periplasm connecting the inner and the outer membranes, are mainly involved in the onset of MDR in Gram-negative bacteria [5, 12–14]. The AcrABZ-TolC efflux pump of *Escherichia coli* is the paradigm model and the most studied RND efflux pump [5]. It is composed of the outer membrane efflux duct TolC, the inner membrane-anchored adaptor protein AcrA, the small transmembrane protein AcrZ and the inner membrane RND protein AcrB [15]. The lattermost protein is a drug/H^+ antiporter fuelled by the proton gradient across the inner membrane and involved in the recognition and translocation of a very broad range of compounds [16].

The multi-drug recognition capabilities and the postulated efflux mechanism of RND transporters are linked through an intriguing structural puzzle, which raised the question of how these proteins achieve their special features. An important step in this direction was made with the publication of the AcrB structure (Fig. 1A), first solved as a symmetric and later as an asymmetric homotrimer [17–20]. The asymmetric structure was postulated to represent the active state of the transporter and featured different conformations of each monomer,

* Corresponding author.
E-mail address: vargiu@dsf.unica.it (A.V. Vargiu).

https://doi.org/10.1016/j.bbagen.2018.01.010
Received 21 September 2017; Received in revised form 28 November 2017; Accepted 11 January 2018
Available online 13 January 2018

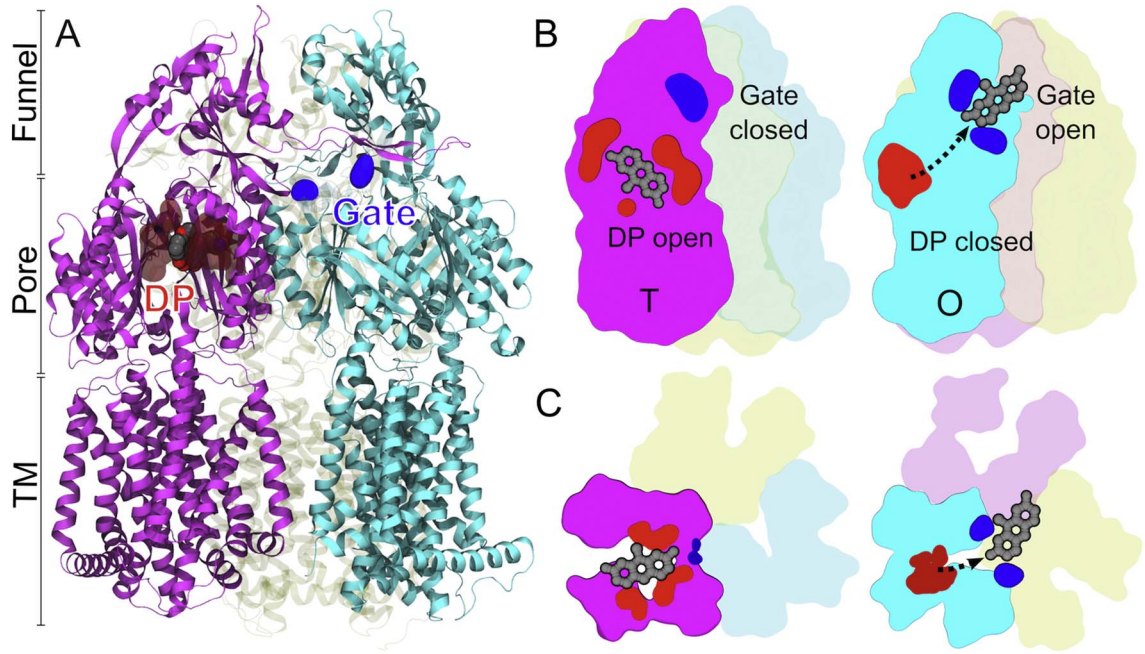

Fig. 1. Structure of AcrB and schematic view of the T → O step of the functional rotation. (A) Overall structure of AcrB (PDB ID:4DX7 [22]). The three main domains (transmembrane - TM, Pore and Funnel) are indicated. Monomers are represented as ribbons, with T and O in front and colored respectively solid magenta and cyan, while L is transparent yellow. A molecule of doxorubicin (DOX) within the DP of monomer T is shown as spheres, with C, O and N atoms colored gray, red and blue respectively. The protein residues within 3.5 Å from DOX are shown as transparent red surfaces. Residues Q124 and Y758 lining the Gate of monomer O are shown as blue solid surfaces. (B) Schematic view of the T → O step of the functional rotation mechanism in AcrB (color code as in A). Left and right pictures represent LTO and TOL conformations respectively. The underlined monomers contain the substrate being transported, and are shown as solid shapes in contrast to the others, which are transparent. The DP and Gate are also shown in the T (left) and O (right) monomers. A model substrate of AcrB is also shown in CPK representation and colored gray. A black dotted arrow on the right picture indicates the direction of transport. (C) Same as in B, but viewed from the top.

named Loose (L), Tight (T), and Open (O) [or, alternatively, Access (A), Binding (B), Extrusion (C)] [17–19]. A "functional rotation" mechanism was proposed explaining substrate export in terms of peristaltic motions induced within the internal channels of the transporter. Recognition of substrates should start at an affinity site, the Access Pocket (AP), in the L monomer [21, 22]. Triggered by substrate binding, a conformational transition from L to T would then occur, accompanied by tight binding of the substrate within a deeper site, the so-called Deep or Distal Pocket (DP) [17–19]. A second conformational change from T to O (supposed to be the energy-requiring step [23]) should drive the release of the substrate towards the upper (Funnel) domain through a putative exit gate (hereafter, simply Gate [19]) (Fig. 1B).

After substrate release, the O conformation would relax back to L (coupled to proton liberation in the cytosol), thus restarting the cycle. Note that different mechanisms of recognition were proposed for high vs. low molecular mass compounds, involving binding to the AP of monomer L and to the DP of monomer T, respectively [21].

The feasibility of the functional rotation mechanism at a molecular level, however, remains to be established. Indeed, while the need for concerted conformational changes of AcrB monomers was demonstrated by several experiments [24, 25], no study addressed so far if and how the transport of substrates occurs through the proposed mechanism. In fact, neither the molecular determinants nor the energetics of the process have yet been thoroughly elucidated. Direct inspection of the functional rotation mechanism at an atomic level will ultimately provide a better understanding of how RND-type transporters work, possibly shedding light on rules governing polyspecific transport and offering precious information for antibacterial drug discovery. In particular, the knowledge of the mechanistic details of the LTO → TOL step of the functional rotation (the underline indicates the monomer transporting the substrate; hereafter T → O) would represent a key milestone. Indeed, wherever recognition occurs, substrates should transit through the DP and the Gate in order to reach the Funnel domain of AcrB [17, 18, 21, 26].

Access to atomistic dynamics of complex molecular machines can be achieved nowadays by means of computer simulations, which represent an alternative and complementary approach to biochemical, biophysical, and structural experiments [27–34]. Since obtaining high-resolution structures of the complexes between RND transporters and known "good" substrates proved to be very challenging [12], it is particularly important to develop computational protocols able to understand mechanisms such as those involved in the extrusion of substrates by these efflux pumps [35, 36].

A few computational studies investigated in part the functional rotation mechanism in AcrB by using either enhanced-sampling all-atom molecular dynamics (MD) simulations [37–41] or a coarse-grained representation of the protein and its substrates [42, 43]. While these studies provided the first insights into the link between conformational changes in the protein and translocation of substrates, they were limited in scope. Specifically, the coarse-grained approaches employed to study RND transporters used a single bead to represent each amino acid in the protein, thus they cannot dissect the role of different atomic-level interactions occurring along the translocation pathways of the substrates. In particular, they cannot address the role of water in the process, which is likely to be important for translocation as substrate diffusion channels are filled with solvent. Regarding the all-atom simulations performed to date: i) they were relatively short considering the size of the system under study, and ii) the conformational changes in the protein and the translocation of compounds were considered as decoupled. These limitations hampered a quantitative understanding of how the former process drives the latter. Most importantly, to our knowledge no study evaluated to date the energetics associated with the diffusion of compounds from the DP to the Funnel domain of AcrB during the T → O conformational change. Thus, it remains to be elucidated how the functional rotation mechanism facilitates the diffusion of substrates of RND transporters.

Prompted by these considerations, we developed a computational protocol based on multiple-bias MD simulations to characterize, for the first time, the key step T → O of the functional rotation mechanism, assessing its energetics and the role of the solvent in the process. The protocol was employed to study the translocation of doxorubicin (hereafter DOX, which together with minocycline and puromycin, are the only drugs co-crystallized within the DP of AcrB [17, 22, 44]) from the DP to the Funnel domain *driven* by conformational changes occurring in AcrB.

Our results demonstrated the effectiveness of the functional rotation mechanism in enabling smooth transport of substrates. The peristaltic motions occurring within internal channels of AcrB enabled the formation of a water layer wetting the internal surface of the translocation channel. This, in turn, permitted a fairly constant hydration of DOX during transport. The mediating action of water leveled off the free energy profile associated to the displacement of the substrate. We speculate that the above mechanism can be generalized to rationalize the transport of substrates other than DOX, and that the mediating action of water is crucial for polyspecific transport by AcrB. Plausibly, other multi-drug transporters could exploit a very similar mechanism to perform their biological functions.

2. Materials and methods

2.1. Simulated system

The system under study has been described in detail earlier [37]. The starting structure consisted of a molecule of DOX bound to the DP of monomer T of the asymmetric homotrimeric AcrB, and was taken from the equilibrium dynamics reported in [37]. The protein was embedded in a 1-Palmitoyl-2-Oleoyl-PhosphatidylEthanolamine (POPE) membrane bilayer model, and the whole system was solvated with a 0.15 M aqueous KCl solution. The total number of atoms in the system was ~450,000.

The parameters of DOX (freely available at http://www.dsf.unica.it/translocation/db [45]) were taken from the GAFF force field [46] and generated using the tools of the AMBER 14 package [47]. In particular, atomic restrained electrostatic potential (RESP) charges were derived using antechamber, after a structural optimization performed with Gaussian09 [48]. The force field for POPE molecules was taken from [37]. The AMBER force field parm14SB [49] was used for the protein, the TIP3P [50] model was employed for water, and the parameters for the ions were taken from [51].

2.2. Computational protocol

In order to mimic DOX translocation from the DP to the Funnel domain in response to the T → O conformational transition of AcrB, we devised an original computational protocol that couples two well-established methods to enhance the sampling of biological processes. Namely, the conformational changes occurring in AcrB were simulated by means of targeted MD (TMD) [52]. This technique mimics structural rearrangements involving large protein regions by applying, to selected atoms (Cαs in our simulations), a force proportional to their displacement from a linear path connecting the initial and final structures. DOX translocation from the DP to the Funnel domain within AcrB was induced by steered MD (SMD), in which one end of a virtual spring is attached to the molecule and the other end is pulled along a predefined direction [53, 54].

Importantly, we mimicked the conformational change of the protein *while* pulling the substrate towards its putative path. To the best of our knowledge, these two computational methodologies have never been combined to date. The resulting DOX translocation pathway was discretized into several snapshots used as starting conformations to perform 1D and 2D umbrella sampling (US) MD simulations [55, 56]. Finally, the weighted histogram analysis method (WHAM) [57] was used to estimate the free energy profile associated to the transport of DOX from the DP to the rear of the Gate. Simulations were analyzed with in-house *tcl*, *bash* and *perl* scripts, with the *cpptraj* tool of the AMBER 14 package [47], and with tools of the GROMACS 5.1.4 package [58]. Figures were prepared using the softwares xmgrace, gnuplot and VMD 1.9.2 [59].

2.2.1. Targeted and steered MD simulations

These simulations (Table S1) were performed using the NAMD 2.9 package [60]. A time step of 1.5 fs was used to integrate the equations of motion. Periodic boundary conditions were employed, and electrostatic interactions were treated using the particle-mesh Ewald method, with a real space cutoff of 12 Å and a grid spacing of 1 Å per grid point in each dimension. The van der Waals energies were calculated using a smooth cutoff (switching radius 10 Å, cutoff radius 12 Å). MD simulations were performed in the NPT ensemble. The temperature was maintained around 310 K by applying Langevin forces to all heavy atoms, with a damping constant of $5\,ps^{-1}$. The pressure was kept at 1 atm using the Nosé-Hoover Langevin piston pressure control with default parameters.

TMD [52] simulations allowed mimicking the conformational transitions between the two known conformational states (LTO and TOL) of AcrB. It was recently shown that TMD simulations produce reliable transition paths as compared to other more refined techniques [61]. To prevent any steric hindrance induced on the T monomer by the neighbors, we targeted all of them towards their next state along the functional rotation cycle. Furthermore, to allow for the largest conformational freedom of the protein along the pathway traced by the targeting restraints, these were applied only to the Cα atoms of AcrB. The force constant was set to $1\,kcal{\cdot}mol^{-1}{\cdot}Å^{-2}$ for each carbon atom, much lower than that employed in earlier studies [37, 40].

Regarding SMD simulations [53, 54], a relatively low force constant ($1\,kcal{\cdot}mol^{-1}{\cdot}Å^{-2}$) was applied to the center of mass of the non-hydrogenous atoms of the substrate. This choice allowed the molecule deviating from a straight pathway and optimizing interactions with the surrounding environment during transport.

2.2.2. Umbrella sampling simulations

To estimate the energetics associated with the translocation of DOX we performed extensive 1D and 2D US simulations [55, 56] along the pathway from the DP to the rear of the Gate (corresponding to a displacement of about 35 Å). The pseudo reaction coordinate used for the evaluation of the free energy profile is different from that used to plot data from the targeted/steered MD simulations. Indeed, in the former simulations we calculated the force as a function of d_{rel}, the distance traveled by the center of mass of the substrate with respect to its initial position. The free energy profile was plotted instead as a function of $d_{Funnel\text{-}DP}$, defined as the difference $d_{DOX\text{-}Funnel}$ - $d_{DOX\text{-}DP}$ between the distance of the center of mass of DOX from the centers of mass of the Funnel domain and of the DP. This choice provides a finer grid for the evaluation of the free energy profile. The path of DOX was discretized into 35 windows covering a $d_{Funnel\text{-}DP}$ range of about 50 Å and placed at 1.5 Å from each other, starting at $d_{Funnel\text{-}DP}$ = 38.0 Å (Table S2). The force constant k_d used to restrain the sampling of DOX within each window along $d_{Funnel\text{-}DP}$ was set to $5\,kcal{\cdot}mol^{-1}{\cdot}Å^{-2}$. 4 additional windows were considered to obtain uniform sampling across the pathway, namely at values of $d_{Funnel\text{-}DP}$ of −9.2, −1.8, 28.3 and 34.3 Å.

Since the orientation of DOX changed near the Gate (namely at values of $d_{Funnel\text{-}DP}$ between ~5 Å and ~12 Å; see Fig. S1), a single reaction coordinate could be insufficient to evaluate the free energy profile correctly. Therefore, a 2D free energy surface was evaluated in that region by introducing the additional angular variable $a_{DOX/Funnel\text{-}DP}$. This is defined as the angle between the main axis of DOX (approximately identified by the line connecting two atoms of the tetracyclic body of the molecule) and the line connecting the centers of mass of the DP and of the Funnel domain (Fig. S2). A total of 28 simulations, each

of 25 ns in length, were performed on a grid defined by points of coordinates ($d_{Funnel\text{-}DP}$, $a_{DOX/Funnel\text{-}DP}$) = ({6.5, 8, 9.5, 11} Å, {60, 75, 90, 105, 120, 135, 150}°). The same value of k_d as in the 1D US simulations was used to restrain the sampling along $d_{Funnel\text{-}DP}$, while a force constant k_a of 120 kcal·mol^{-1}·rad^{-2} was used to restrain the orientation of the substrate.

The values of $d_{Funnel\text{-}DP}$ and $a_{DOX/Funnel\text{-}DP}$ were saved every 2 ps (corresponding to 1333 simulation steps). The WHAM method [57] as implemented in the *g_wham* tool of GROMACS was used to extract the free energy profiles and surfaces, using a tolerance of 10^{-6} for the convergence of the probability. Simple Bayesian bootstrapping was utilized to estimate the statistical sampling errors using 500 randomly chosen data sets with the same data size.

The RMSD of the complexes with respect to their initial conformation revealed minor structural changes in all windows (Fig. S3A). A fairly flat profile was indeed reached after ~20 ns. In addition, the orientation of DOX did not change significantly in any of the 1D US windows (Fig. S3B). The relatively good stability of the systems was mirrored in the fairly good convergence of the free energy profile (Fig. S3C). The free energy profile (surface) presented in the following section 3 Results and discussion was estimated over the last 12.5 (6.25) ns of the simulation.

3. Results and discussion

In this section we discuss our main results, describing the structural, dynamical and energetic features of the functional rotation mechanism and comparing them with the available experimental data. Finally, we thoroughly validate and assess the limitations of our computational protocol.

3.1. Mimicking the functional rotation mechanism in silico

By efficiently coupling TMD and SMD simulations techniques we aimed to thoroughly mimic the functional rotation *in silico*, thus simulating substrate translocation *driven* by the structural changes of AcrB. In order to achieve this goal, we first addressed a key issue concerning the coupling times between protein conformational changes and substrate translocation. Indeed, different substrates could "respond" (i.e. unbind from the DP) with different timings to the conformational changes in the RND transporter, due e.g. to their different binding affinities, sizes, etc. Moreover, we do not know a priori the details of such process even for a single substrate, including DOX.

To cope with this issue, we simulated different possible couplings between the two processes. Namely, we performed three simulations in which DOX was pulled from the DP towards the Funnel domain in 1 μs, while the T → O conformational transitions in AcrB were induced respectively within the first 0.1, 0.2, and 0.3 μs (Table S1). Hereafter, we refer to these simulations as $T_{rot}\_10\%T_{pull}$, $T_{rot}\_20\%T_{pull}$ and $T_{rot}\_30\%T_{pull}$, respectively. In addition, we performed a 1 μs long SMD simulation without concomitant induction of conformational changes in AcrB (referred to as $T_{pull\_1\mu s}$). Though not representative of any putative transport mechanism in AcrB, the $T_{pull\_1\mu s}$ simulation is very useful for comparative purposes. Overall, the translocation of DOX as seen in our simulations turns out to be quite unaffected by the details of the computational setup, *as far as the conformational changes of the protein are mimicked concomitantly to the displacement of the substrate* (Fig. 2).

3.2. The transport mechanism is consistent with experimental data

First, we validated our computational protocol by assessing the consistency of the mechanism of substrate translocation *in silico* with the available experimental data. Importantly, the substrate is always transported through the putative Gate of AcrB (Fig. 2A–B and Movie S1).

More generally, during translocation DOX interacts with protein residues suggested experimentally [62] to be part of the extended DP and of the putative Gate (Fig. 2C and Table S3). Being an extension of the vast and malleable DP, the path towards the Gate allows for consistent substrate rearrangement, as documented by the change in the orientation of DOX observed in all simulations (Fig. S1 and Movie S1). Previous experimental data demonstrated that DOX binds to the DP of AcrB assuming almost flipped orientations [17, 22] (Fig. S4). Our results show that rotation of the substrate is possible also during its transport, at least within the channel leading from the upper part of the DP to the Gate. Importantly, such reorientation of DOX occurs at almost no cost (see below).

3.3. Functional rotation enables continuous substrate hydration during transport

The overall agreement among the main results obtained from $T_{rot}\_10/20/30\%T_{pull}$ simulations discussed above is congruous with the resemblance of the profiles of the pulling force F_{pull} applied to induce the translocation of DOX (Fig. 2D). Note that all profiles are relatively smooth and do not feature large values of F_{pull}, which would be associated with transport bottlenecks. In particular, there is no evidence for high values of F_{pull} near the Gate. On the contrary, a prominent peak of almost 10 kcal·mol^{-1} Å^{-1} in F_{pull} appears near this region when the translocation of DOX is mimicked in the complete absence of conformational changes in AcrB, i.e., for $T_{pull\_1\mu s}$ (Fig. 2D). Thus, the T → O conformational change facilitates substrate translocation.

In order to shed light on the microscopic determinants of the process, we performed a detailed analysis of the interactions involving DOX, the protein and the solvent. As expected, in the absence of the T → O conformational change, the passage of DOX through the Gate induces a clear structural strain in the substrate (Fig. 3). More importantly, the opening of the Gate following the T → O transition enables a fairly structured hydration of almost the entire internal surface of the translocation channel leading from DP to the Funnel domain (Fig. 4).

This is particularly evident from the plot of the spatial distribution function (SDF) of water molecules (Fig. 4A), which provides a picture of the order in liquid water and reveals specific details of its local structure [63]. Note that structured hydration of the translocation path is compatible with the relatively hydrophilic character of the channel connecting the DP to the Funnel domain (Table S4, and see also [40]).

By comparing the hydration properties of the translocation channel and of the substrate in $T_{pull}\_10\%T_{rot}$ and $T_{pull\_1\mu s}$ simulations, it is clear that this phenomenon is a peculiar feature of the functional rotation mechanism (Fig. 4). As a consequence of the reduced screening effect of waters in $T_{pull\_1\mu s}$, a negative peak appeared in the corresponding DOX-AcrB interaction energy profile (Fig. 4B and Fig. S5). The presence of an almost continuous layer of waters within the translocation channel enables a fairly constant wetting of the substrate, as well as the establishment of several water-mediated interactions with the protein (Fig. 4B).

3.4. Substrate translocation occurs over a smooth free energy profile

To quantitatively address to what extent the functional rotation mechanism does promote the diffusion of substrates, we performed US simulations [55, 56] (Tables S1 and S2) to estimate the free energy profile associated with the transport of DOX from the DP to the rear of the Gate (Fig. 5), that is the part of the translocation process occurring within the AcrB channel (corresponding to a change of about 35 Å in the relative displacement from the DP, d_{rel}). The profile is relatively smooth, with barriers lower than 5 kcal·mol^{-1}. Furthermore, the affinities of DOX to the DP and the Gate are virtually identical (Fig. 5A); thus, the probability to find the substrate near the second site increases in response to conformational cycling in AcrB.

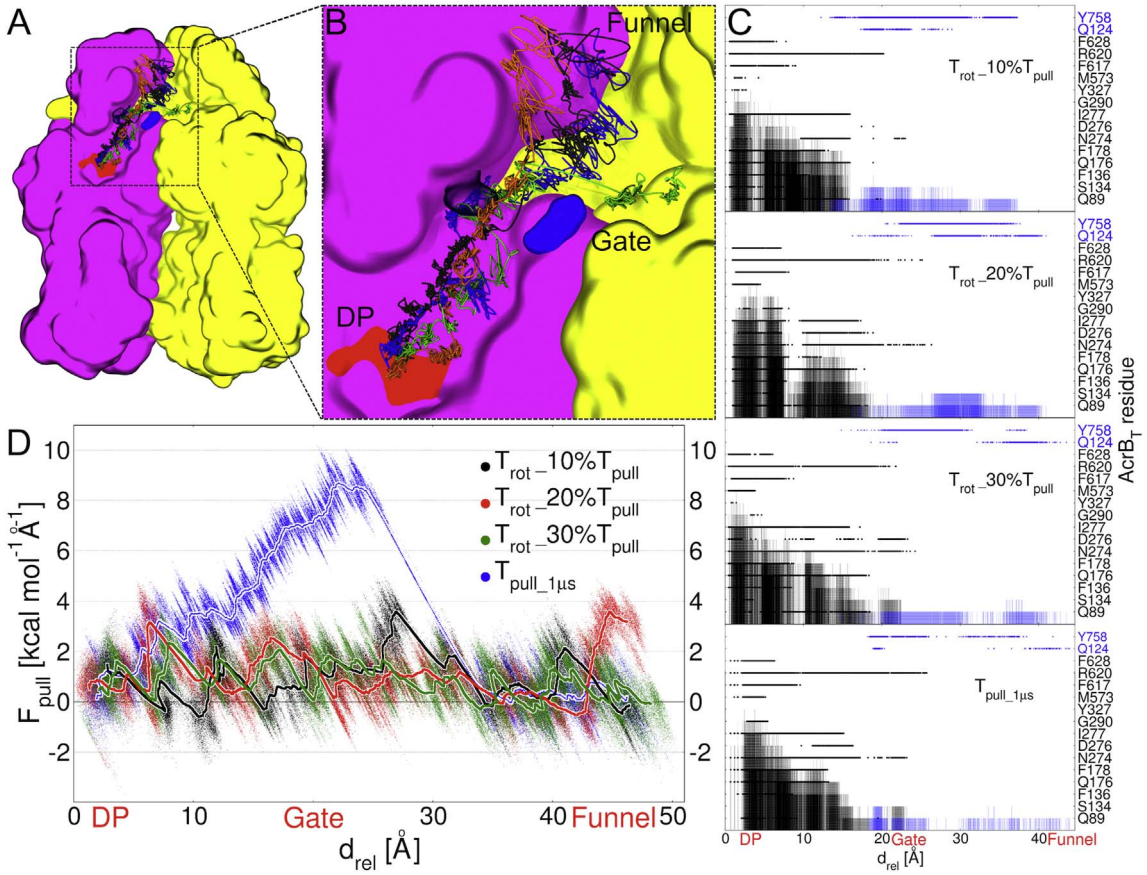

Fig. 2. Translocation of DOX during the T → O step of the functional rotation in AcrB. (A) Overall view of translocation pathways from the DP to the Gate as seen in multi-bias MD simulations labeled T_{rot}_10%T_{pull}, T_{rot}_20%T_{pull} and T_{rot}_30%T_{pull} and in the SMD simulation T_{pull}_1μs. For clarity, only monomers T and L of AcrB are shown in magenta and yellow surfaces, respectively. In addition, some regions of the monomer T were removed to allow visualizing the transport pathways. Part of the DP within monomer T is colored red. Residues Q124 and Y758 lining the Gate are shown as solid and transparent blue surfaces, respectively. Black, red, green and blue solid lines indicate pathways of DOX in T_{rot}_10%T_{pull}, T_{rot}_20%T_{pull}, T_{rot}_30%T_{pull} and T_{pull}_1μs, respectively. (B) Magnification of the region within the square dotted box in A. (C) Plots of the per-residue (dots) and cumulative (semi-transparent bars) contacts between DOX and residues identified as those lining the substrate transport pathway in AcrB [62]. The x-axis reports the displacement d_{rel} of DOX with respect to its initial position within the DP. Black and blue labels indicate residues lining the DP and the Gate, respectively. A contact was recorded at each step if the minimum distance of DOX from any residue was lower than 3 Å. (D) Profiles of F_{pull} extracted from T_{rot}_10%T_{pull}, T_{rot}_20%T_{pull}, T_{rot}_30%T_{pull} and T_{pull}_1μs. Tiny points and thick lines indicate forces calculated every 2000 steps of MD simulation and running averages over 5000 points, respectively.

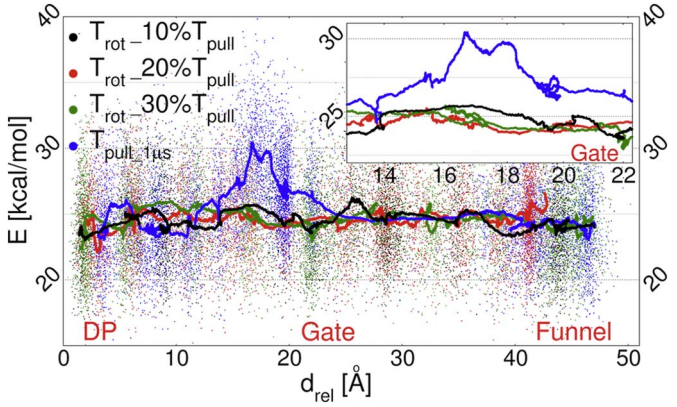

Fig. 3. Conformational strain experienced by DOX during transport. Plots of the internal energy of DOX (calculated from the dihedral energy terms of the force field) calculated from simulations T_{rot}_10%T_{pull}, T_{rot}_20%T_{pull}, T_{rot}_30%T_{pull} and T_{pull}_1μs. Tiny points and lines indicate forces calculated every 2000 steps of the MD simulation and running averages over 5000 points, respectively. The inset shows the region of higher discrepancy between the profile from T_{pull}_1μs and all the others.

Since the orientation of DOX along its translocation path changes near the Gate (inset in Fig. 5B, and Fig. S1), we included an angular variable $a_{DOX/Funnel\text{-}DP}$ (representing DOX rotation) to estimate the 2D free energy profile in the corresponding region of the translocation process (Fig. 5C). Importantly, the addition of $a_{DOX/Funnel\text{-}DP}$ had a very small impact on the results discussed above. Indeed, both the free energy difference found between the states representing almost flipped orientations of DOX (labeled 3 and 4 in Fig. 5A) and the barrier associated with the rotation remain vanishingly small.

3.5. Biological implications

In this section we discuss further the possible implications of our findings in relation to the current view of how RND efflux pumps work. The proposals below could be of inspiration for additional computational and experimental studies.

3.5.1. AcrB substrates can adopt multiple binding modes also outside the DP

We showed that DOX assumes different orientations during transport. While such rotation can be facilitated by the increased hydration of DOX upon detachment from the DP (Fig. 4B), we cannot exclude the presence of multifunctional sites (that is, sites able to recognize various types of functional groups, from hydrophobic to polar and charged) within the channel leading from this site to the Gate. Note that the presence of such multifunctional sites has been demonstrated within the DP [64, 65], and is coherent with the possibility for DOX to adopt (at least) two different orientations in that site [17, 22]. A new possibility arising from our findings is that multidrug recognition and

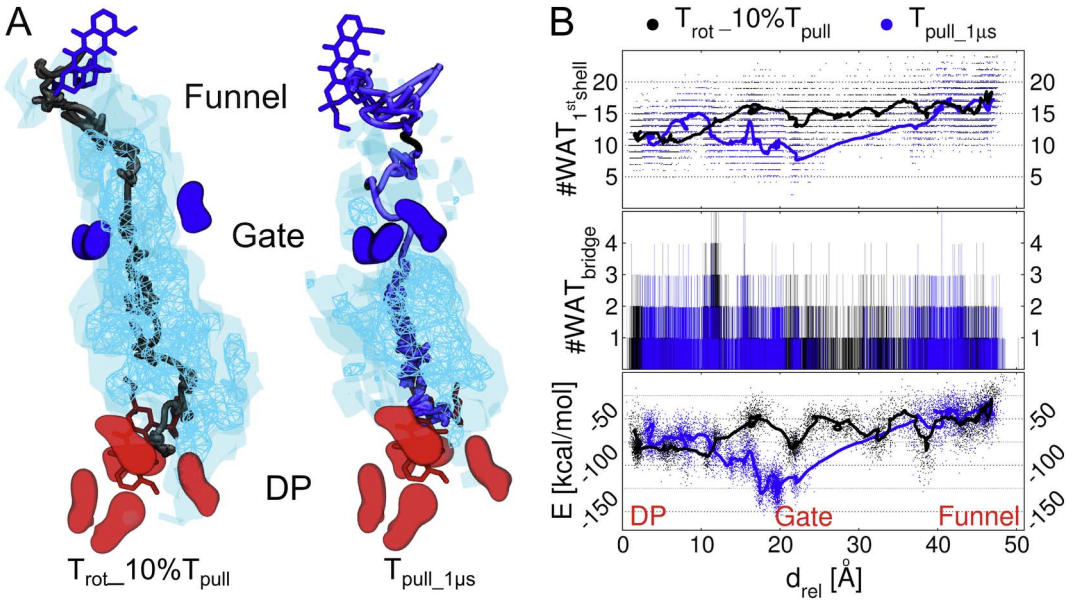

Fig. 4. The functional rotation mechanism enables continuous hydration of the transport channel and of the substrate. (A) SDF isosurfaces of water oxygen atoms within the transport channel leading from the DP to the Funnel domain. Left and right pictures refer to simulations $T_{rot}\_10\%T_{pull}$ and $T_{pull\_1\mu s}$, respectively. The positions of DOX at the beginning and at the end of the simulations are shown as red and blue sticks, respectively. The pathways traced by the center of mass of the drug (sampled every 2.5 ns) in $T_{rot}\_10\%T_{pull}$ and $T_{pull\_1\mu s}$ are displayed as dark gray and light blue tubes respectively. SDF surfaces corresponding to isovalues of 5 and 1 (with respect to the average value in bulk water) are shown as cyan nets and transparent surfaces, respectively. (B) DOX hydration properties and interaction with AcrB during transport in $T_{rot}\_10\%T_{pull}$ and $T_{pull\_1\mu s}$. Upper graph: number of water molecules within the first hydration shell of DOX as a function of d_{rel}. Middle graph: number of water-bridged interactions between DOX and the protein. Lower graph: profiles of AcrB-DOX interaction energy calculated from the force-field terms representing electrostatics and van der Waals interactions. Tiny points and lines in the upper and lower graphs indicate respectively values calculated every 2000 steps and running averages over 5000 points. See Fig. S5 for a comparison including also $T_{rot}\_20\%T_{pull}$ and $T_{rot}\_30\%T_{pull}$.

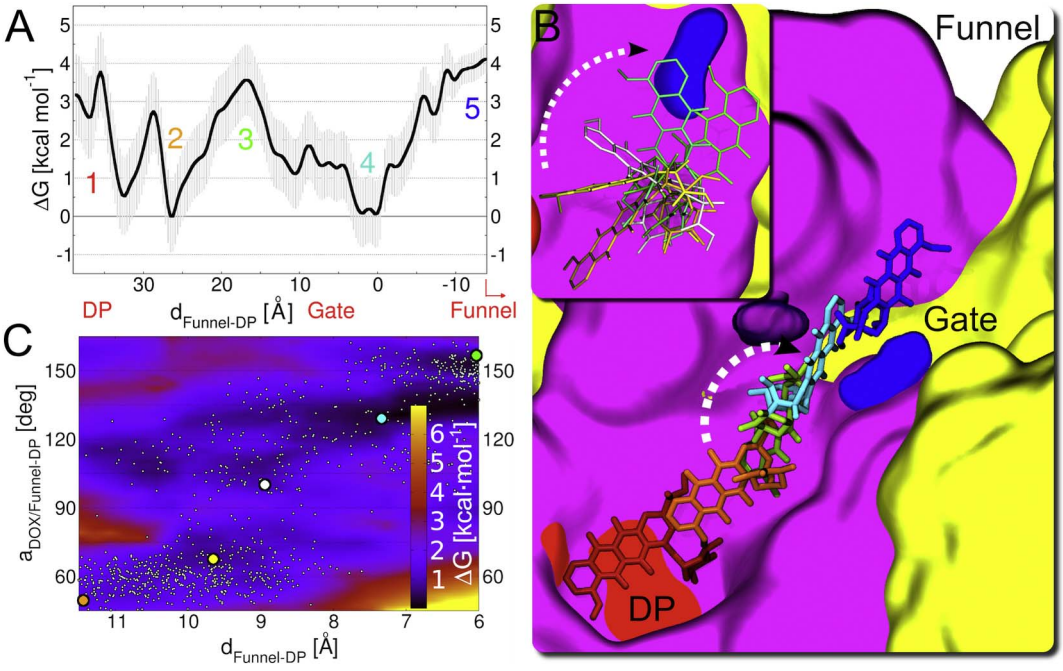

Fig. 5. Energetics of DOX transport within AcrB. (A) 1D free energy profile associated to transport of DOX from the DP to the rear of the Gate along the T → O step of the functional rotation. The profile of ΔG (kcal·mol^{-1}) referred to the binding free energy within the DP is reported as a function of the pseudo reaction coordinate $d_{Funnel\text{-}DP}$, defined as the difference in the distance of DOX from the center of the Funnel domain and from the center of the DP (see Materials and Methods). Colored numbers in the graph identify arbitrary stages of the transport process, for which the conformation of DOX is shown in B with the same color code. (B) Representative conformations of DOX along the translocation pathway as seen in the $T_{rot}\_10\%T_{pull}$ simulation. DOX conformations are shown as sticks of different colors, representing different stages of the process and corresponding to positions identified by numbers 1 to 5 in A. The protein, the DP and the Gate are represented as in Fig. 2A. Inset: detailed view of the rotation of DOX near the Gate. Selected conformations are shown as thin sticks colored as the large points in C. (C) 2D free energy profile as a function of $d_{Funnel\text{-}DP}$ and of the angle $a_{DOX/Funnel\text{-}DP}$, calculated in the region where the change in orientation of DOX occurs (see Fig. S1). Colored points indicate conformations of DOX extracted from the $T_{rot}\_10\%T_{pull}$ simulation and featuring different orientations, and shown with the same color code in the inset of B.

transport are not restricted to one or more binding sites (e.g. the DP), but rather dictated by the physico-chemical properties of the *entire* substrate translocation pathway through AcrB. These findings are compatible with polyspecific transport by AcrB.

3.5.2. A "one stroke - one drug" mechanism of substrate expulsion is not necessary for AcrB

As a result of the T → O conformational change in AcrB, the interaction strength of DOX with the Gate and with the DP become comparable (Fig. 5A). Thus, the functional rotation mechanism could contribute to efflux by "just" favoring the accumulation of substrates in the central region of the upper Funnel domain, beyond the Gate. This should create a concentration gradient between this region and the end of the AcrA/TolC channel, driving the translocation of a pile of compounds through the latter pathway, as hypothesized earlier [23]. Such a mechanism may explain how certain substrates (e.g. aminoacyl-β-naphthylamides [66]) are pumped out at rates far exceeding those expected for common transporters, suggesting that many substrate molecules might be pushed out in one stroke.

The largely prevalent hydrophilic character identified in the internal surfaces of MexA and OprM (respectively homologous of AcrA and TolC in *Pseudomonas aeruginosa*) [67] further corroborates our hypothesis. Moreover, an analysis of the hydrophilic character of the internal surfaces of AcrA and TolC in the recently published structure of the complete AcrABZ-TolC assembly [68] confirmed these findings (Fig. S6). Therefore, it is plausible that upon crossing the Gate, AcrB substrates will float within an environment that would favor their extrusion.

3.5.3. Transport rate bottleneck is not due to diffusion of substrates within AcrB

The smooth free energy profile associated with the translocation of DOX implies that the bottleneck in terms of rate of transport comes from the concerted conformational changes occurring in AcrB. This hypothesis is in line with the current understanding of how many active transporters work [69], and it is supported by the comparison of our data with experimental studies reporting AcrB efflux rates of several compounds [70–72]. For instance, the values of the turnover number k_{cat} estimated by Nikaido and co-workers [70, 71] for the efflux of cephalosporins and penicillins range from $\sim 10\,s^{-1}$ to $\sim 10^3\,s^{-1}$. Using simple arguments from transition state theory to get an approximate value of the effective free energy barrier $\Delta G^{\ddagger}$ that would be compatible with this rate, we obtained $\sim 13\,kcal{\cdot}mol^{-1}$, which is well above the highest barrier reported here. Interestingly, the effective free energy barrier calculated for the translocation of DOX through the TolC channel amounted to almost $10\,kcal{\cdot}mol^{-1}$ [73], a value similar to those extrapolated from the experimental data on efflux kinetics [70, 71]. Finally, surface plasmon resonance experiments on the interaction of substrates with AcrB only concluded that the rates of binding and unbinding were too fast for kinetic modeling [74, 75]. These findings are consistent with our results, which highlight the key effect of the conformational changes in AcrB in lowering the barriers for substrate diffusion, and support the hypothesis that diffusion of substrates out of this transporter is associated with relatively high free energy barriers. Such barriers could perhaps be effectively reduced by increasing the local concentration of compounds at the AcrA/AcrB interface, a hypothesis in line with the above discussion about efflux rate bottlenecks.

3.5.4. Water is key for polyspecific transport by AcrB

According to our results, the relief of steric hindrance and the formation of a continuous layer of structured waters crucially facilitate substrate transport inside AcrB. The mechanism we propose would: *i*) match with the increasing ratio of hydrophilic over hydrophobic residues along the channel leading from the DP to the Funnel domain [40]; *ii*) be compatible with the many structural waters found within internal surfaces of AcrB in the highest-resolution crystal structure reported to date (PDB ID 4DX5 [22]).

Moreover, it is likely that this very general mechanism would facilitate diffusion of several chemically unrelated substrates dissociating from the DP, thus enabling polyspecific transport. Indeed, by shielding potentially (too) strong interactions between chemical groups of compounds and AcrB, water would in part "hide" chemical differences among diverse substrates. Therefore, translocation of neutral, zwitterionic, anionic and cationic compounds could occur along a similar path and with comparable overall costs. Although verifying such a hypothesis with other compounds would be very computationally demanding, we point out that among the drugs co-crystallized so far within the DP of AcrB (including minocycline [17, 22] and puromycin [44]), DOX features overall the largest molecular mass, van der Waals volume and minimal projection area (see e.g. data at www.dsf.unica.it/translocation/db [45]). Moreover, it is as soluble as the other substrates (all have high solubility in water, the values of intrinsic logS being −3.6, −3.2 and −2.3 for DOX, puromycin and minocycline, respectively according to Chemicalize - https://chemicalize.com). Therefore, it is plausible to expect that compounds smaller than DOX, but of similar solubility, could be transported via the same mechanism described above, although with different kinetics depending also on their binding mode (and strength) to the DP [70, 71, 74, 76, 77]. Note that providing a full molecular interpretation of the data reported by experimental studies on efflux kinetics goes far beyond the scope of this work. Indeed, the kinetic and equilibrium constants measured in [70, 71, 74, 76, 77] involve additional transport processes such as the uptake of drugs by AcrB and the diffusion of compounds through different sites of the transporter and through the whole AcrABZ-TolC pump. Nonetheless, the above considerations strongly suggest that water mediates the transport of (at least) low-molecular mass substrates recognized at the DP.

3.5.5. Recognition and transport of substrates in AcrB

On the basis of our findings and according to previous literature, the mechanism by which AcrB and its homologs proteins recognize and transport their substrates would be as follows:

- Recognition occurs via interaction of substrates with one among the multiple binding sites present in AcrB, each endowed with a few multifunctional sites [17, 21, 22, 26, 65].
- Concerning the DP, the interaction of the substrate with this site triggers the T → O conformational changes in the protein, lowering the affinity of the compound to the pocket.
- Upon unbinding from the DP, the substrate will find itself in a relatively hydrated environment favoring smooth diffusion towards the Gate or, at least, disfavoring specific interactions that could hinder transport. This hypothesis matches with the physico-chemical traits of typical AcrB substrates, whose unique common feature is some degree of lipophilicity [5, 16]. Furthermore, the latter scenario is compatible with the transport of a pile of compounds through repeated conformational cycling of the pump [23].

Note that, according to the mechanism described above, the distinction between a substrate and an inhibitor (or between a good and poor substrate of the pump) could be related to the way they bind to the same region of AcrB (binding strength and/or position), which should induce different rearrangements of the pump (as already suggested by several studies [44, 78–80]) thus affecting transport kinetics [66, 74, 76].

3.6. Validation of the protocol

The robustness of the protocol vs. small variations in the relative coupling times between conformational changes induced in AcrB and displacement of DOX has been discussed above. In the following, we report on an extensive validation of our methodology and a comparison

of our results with previously published computational works.

3.6.1. Robustness of the protocol vs. slight changes in the pulling direction

We compared the dynamics of DOX in two SMD simulations of equal length (namely 35 ns, see Table S1) but assuming slightly different pulling directions. We tested two "natural choices" (Fig. S7A), namely: i) the direction "DP-Gate" leading from the center of mass of DOX in the starting structure (within the DP of monomer T) to the center of mass of the Gate of monomer T; ii) the direction "Funnel-DP" also from the center of mass of DOX to the center of mass of selected atoms of the funnel domain (namely the Cαs of residues 199 to 210 of each monomer). The profiles of F_{pull} turned out to be very similar in the two simulations (Fig. S7B). Since the direction "Funnel-DP" should be less sensitive to conformational changes of AcrB (as the center of mass of this region should not change significantly during the functional rotation), we used that pulling direction in all of the remaining simulations.

3.6.2. Impact of the simulation time on the mechanism and on the energetics of the process

We also investigated how the simulation length affects the translocation process and moreover the profile of the pulling force F_{pull}. Since the relative displacement of DOX from its initial position in the DP amounts to a few nm, pulling too fast could induce artificial strain in both, the substrate and the surrounding amino acids. Such an artifact could lead to discrepancies between the true translocation pathway and the one seen in simulations. In order to quantify this effect, we performed three different SMD simulations of length 10, 100 and 1000 ns. Pulling velocities varied from $\sim 5{\cdot}10^{-3}$ Å·ps^{-1} to $\sim 5{\cdot}10^{-5}$ Å·ps^{-1} in the shortest and longest simulation, respectively (Table S1). An overall comparison of the translocation pathways among the various simulations does not reveal any large difference (unpublished observations), although it turns out that a full translocation is achieved only in the two longest simulations (Fig. S8A). Moreover, the profiles of F_{pull} show many more spikes in the shorter than in the longest simulation. The latter one features a maximum value of F_{pull} significantly lower than the former, clearly located near the Gate. We conclude that, given the size of the system under investigation and the complexity of the process under study, a relatively long simulation (preferably of 1 μs) is necessary to reduce artificial distortions in the structures of the interacting partners.

We further verified the impact of the simulation time by comparing the profiles of F_{pull} among three $T_{rot}\_10\%T_{pull}$ simulations in which T_{pull} was set to 10, 100 and 1000 ns respectively (Fig. S8B). In this case too, the larger is the simulation time, the lower are the average and maximum values of F_{pull}.

The comparison of the profiles of F_{pull} at various simulation times between the steered and the steered/targeted MD simulations (Fig. S8A–B) revealed that the specific computational protocol also plays an important role. In particular, it is evident that the maximum value of F_{pull} found in the shortest $T_{rot}\_10\%T_{pull}$ simulation (where T_{pull} was set to 10 ns) is significantly lower than that found in the longest SMD simulation ($T_{pull\_1\mu s}$).

3.6.3. Comparison with previous computational work

Recently Wang and co-workers compared the translocation mechanisms of DOX and of the inhibitor D13-9001 by performing all-atom TMD simulations of the T → O conformational change to displace the ligands out of the DP, *followed* by SMD simulations to pull the compounds towards the Funnel domain [39]. The overall behavior of DOX during the targeted MD simulations was very similar to that reported by some of us in a previous study [37], despite differences in the initial positions of the ligand. This was to be expected since the length of the simulations performed in [39] is of the same order of magnitude of those reported by us in [37], namely a few tens of ns at most. However, pulling the substrate only once the T → O transition was completed leaded to significant oscillations in F_{pull} (see Fig. S6b in [39]). This behavior is similar to that we have seen in relatively short SMD simulations (Fig. S9).

In order to quantitatively compare our profiles of F_{pull} with that reported by Zuo et al., [39] we plotted our data as a function of the reaction coordinate defined there. They used the inverse of the distance between the mass center of DOX to centroid of the Cα atoms of N747 in the T protomer and D788s in protomers L and O (see the legend of Fig. 4 in [39]). The profile of F_{pull} reported in [39] features a maximum near the Gate, where its value is twice as high as the values in the corresponding region in our profiles (Fig. S9).

Note that extending the simulation time of the two successive (*uncoupled*) simulations (TMD and subsequent SMD) probably does not help recovering a smooth profile of F_{pull}. For instance, we verified (data not shown) that extending the simulation time of the TMD to 100 ns without concomitantly pulling the substrate often resulted in much smaller displacements of DOX compared to those seen in [37, 39]. Moreover, the results were poorly reproducible regarding the displacement of DOX. Therefore, the SMD simulation would begin from significantly different positions of the substrate in the different replicas, likely affecting the overall results. Thus, decoupling TMD from SMD simulations was not a suitable option according to our results. In contrast, the movement of DOX occurring in the first 100 ns of the $T_{rot}\_10\%T_{pull}$ simulation was consistent among three different replicas (Fig. S10). This finding suggests that pulling the substrate while inducing the conformational change in AcrB can generate similar trajectories when using the same setup.

3.7. Limitations of our approach

Clearly, a proper comparison of our results with experiments is flawed by several factors, and in this section we discuss some possible limitations of our computational protocol. First, all-atom classical MD simulations with predefined protonation states of all molecules neglect the coupling between conformational changes occurring in the periplasmic region of AcrB and the flux of protons across the TM domain. However, this limitation will hardly affect the overall outcome, since the translocation of DOX occurs fully within the periplasmic domain. Furthermore, we are mimicking exactly the process (i.e. the LTO → TOL conformational change) induced by the change in the protonation states of key residues within the TM region.

Another limitation of our approach consists in neglecting the AcrB partners forming the full AcrABZ-TolC assembly [44, 68, 81, 82]. In particular, the extrusion process could be affected by the interaction between AcrB and AcrA, which could alter e.g. the flexibility and the hydration properties of the upper part of the Funnel domain. However, we believe that restricting our study to AcrB does not constitute a major drawback, as the translocation of DOX simulated here occurs mainly within internal AcrB channels.

4. Conclusions and perspectives

In this work we developed and validated a novel computational protocol to mimic *in silico* the key step (T → O) of the functional rotation mechanism by which RND transporters such as AcrB are believed to export their substrates. To the best of our knowledge, this is the first computational study: *i*) thoroughly addressing the coupling between the conformational transitions occurring in a RND-type transporter and the translocation of its substrates; *ii*) providing an estimate of the free energy profile associated with the key step of the efflux process, that is the transport of a substrate from the DP to the Funnel domain; *iii*) highlighting the role of structured waters for smooth transport of substrates. Thanks to this unprecedented computational effort, we characterized the molecular determinants of substrate translocation caused by peristaltic-like motions occurring within internal channels of AcrB. Using doxorubicin as a probe we showed how these structural changes favor substrate transport along a path that is fully compatible with that

proposed on the basis of X-ray data and whole cells assays. Moreover, we propose a rationale for the polyspecific transport by the RND-type multidrug efflux pump AcrB, in which water molecules play a key role. Clearly, water-mediated transport could be a general feature of the multidrug transport mechanism.

Accurate computational protocols, such as the one used here, represent a valid and highly informative strategy to understand the molecular mechanisms of recognition and transport by RND proteins. Moreover, given the robustness of the methodology with respect to implementation details, we are confident that it can be successfully applied to study the transport of other substrates by AcrB and homologous proteins, and easily adapted to investigate complex processes in other biological systems.

Abbreviations

AP	Access Pocket
DOX	doxorubicin
DP	Distal Pocket
MD	Molecular Dynamics
MDR	Multi-Drug Resistance
POPE	1-Palmitoyl-2-Oleoyl-PhosphatidylEthanolaminel
RESP	Restrained ElectroStatic Potential
RND	Resistance-Nodulation-cell Division
SDF	Spatial Distribution Function
SMD	Steered Molecular Dynamics
TM	Trans-Membrane
TMD	Targeted Molecular Dynamics
US	Umbrella Sampling
WHAM	Weighted Histogram Analysis Method

Supplementary data to this article can be found online at https://doi.org/10.1016/j.bbagen.2018.01.010.

Transparency document

The http://dx.doi.org/10.1016/j.bbagen.2018.01.010 associated with this article can be found in online version.

Acknowledgments

The research leading to the results discussed here was partly conducted as part of the Translocation Consortium (http://www.translocation.eu) and has received support from the Innovative Medicines Initiative Joint Undertaking under Grant Agreement no. 115525, resources that are composed of financial contribution from the European Union's Seventh Framework Programme (FP7/2007-2013) and EFPIA companies in kind contribution. VKR is a Marie Skłodowska-Curie fellow within the “Translocation” Network, project no. 607694. This research used the Savio computational cluster resource provided by the Berkeley Research Computing program at the University of California, Berkeley (supported by the UC Berkeley Chancellor, Vice Chancellor for Research, and Chief Information Officer). We thank H. Nikaido (University of California at Berkeley, USA), K.M. Pos (Goethe University, Frankfurt am Main, Germany), H. Zgurskaya (University of Oklahoma, Norman, OK, USA), M. Picard (CNRS/Université Paris-Diderot, Paris, France), E. Bibi (Weizmann Institute of Science, Rehovot, Israel), J. Blair and L. Piddock (University of Birmingham, UK), C. Melis (University of Cagliari, Italy), F. Pietrucci (Université Pierre et Marie Curie, Paris, France) and A. Kranjc for the critical reading of the manuscript.

Author contributions

A.V.V., U.K., and P.R. conceived and designed research. A.V.V. performed research. A.V.V. and P.R. analyzed the data. A.V.V., V.K.R., I.M., and G.M. contributed materials and analysis tools. All authors wrote the manuscript.

Competing interests

The authors declare that they have no competing interests.

References

[1] K. Hede, Antibiotic resistance: an infectious arms race, Nature 509 (2014) S2–S3.
[2] E.D. Brown, G.D. Wright, Antibacterial drug discovery in the resistance era, Nature 529 (2016) 336–343.
[3] P. Courvalin, Why is antibiotic resistance a deadly emerging disease? Clin. Microbiol. Infect. 22 (2016) 405–407.
[4] H. Inoue, R. Minghui, Bulletin of the World Health Organization, vol. 95, (2017), p. 242.
[5] X.-Z. Li, P. Plésiat, H. Nikaido, The challenge of efflux-mediated antibiotic resistance in gram-negative bacteria, Clin. Microbiol. Rev. 28 (2015) 337–418.
[6] J.M.A. Blair, G.E. Richmond, L.J.V. Piddock, Multidrug efflux pumps in gram-negative bacteria and their role in antibiotic resistance, Future Microbiol 9 (2014) 1165–1177.
[7] J. Sun, Z. Deng, A. Yan, Bacterial multidrug efflux pumps: mechanisms, physiology and pharmacological exploitations, Biochem. Biophys. Res. Commun. 453 (2014) 254–267.
[8] S. Hernando-Amado, P. Blanco, M. Alcalde-Rico, F. Corona, J.A. Reales-Calderon, M.B. Sanchez, J.L. Martinez, Multidrug efflux pumps as main players in intrinsic and acquired resistance to antimicrobials, Drug Resist. Updat. 28 (2016) 13–27.
[9] M. Chitsaz, M.H. Brown, The role played by drug efflux pumps in bacterial multidrug resistance, Essays Biochem. 61 (2017) 127–139.
[10] N. Tal, S. Schuldiner, A coordinated network of transporters with overlapping specificities provides a robust survival strategy, Proc. Natl. Acad. Sci. U. S. A. 106 (2009) 9051–9056.
[11] G. Zhou, Q.-S. Shi, X.-M. Huang, X.-B. Xie, The three bacterial lines of defense against antimicrobial agents, Int. J. Mol. Sci. 16 (2015) 21711–21733.
[12] A. Yamaguchi, R. Nakashima, K. Sakurai, Structural basis of RND-type multidrug exporters, Front. Microbiol. 6 (2015) 327.
[13] H.I. Zgurskaya, J.W. Weeks, A.T. Ntreh, L.M. Nickels, D. Wolloscheck, Mechanism of coupling drug transport reactions located in two different membranes, Front. Microbiol. 6 (2015) 100.
[14] K. Poole, Efflux pumps as antimicrobial resistance mechanisms, Ann. Med. 39 (2007) 162–176.
[15] D. Du, H.W. van Veen, B.F. Luisi, Assembly and operation of bacterial tripartite multidrug efflux pumps, Trends Microbiol. 23 (2015) 311–319.
[16] P. Ruggerone, S. Murakami, K.M. Pos, A.V. Vargiu, RND efflux pumps: structural information translated into function and inhibition mechanisms, Curr. Top. Med. Chem. 13 (2013) 3079–3100.
[17] S. Murakami, R. Nakashima, E. Yamashita, T. Matsumoto, A. Yamaguchi, Crystal structures of a multidrug transporter reveal a functionally rotating mechanism, Nature 443 (2006) 173–179.
[18] M.A. Seeger, A. Schiefner, T. Eicher, F. Verrey, K. Diederichs, K.M. Pos, Structural asymmetry of AcrB trimer suggests a peristaltic pump mechanism, Science 313 (2006) 1295–1298.
[19] G. Sennhauser, P. Amstutz, C. Briand, O. Storchenegger, M.G. Grütter, Drug export pathway of multidrug exporter AcrB revealed by DARPin inhibitors, PLoS Biol. 5 (2007) e7.
[20] S. Murakami, R. Nakashima, E. Yamashita, A. Yamaguchi, Crystal structure of bacterial multidrug efflux transporter AcrB, Nature 419 (2002) 587–593.
[21] R. Nakashima, K. Sakurai, S. Yamasaki, K. Nishino, A. Yamaguchi, Structures of the multidrug exporter AcrB reveal a proximal multisite drug-binding pocket, Nature 480 (2011) 565–569.
[22] T. Eicher, H.-J. Cha, M.A. Seeger, L. Brandstaetter, J. El-Delik, J.A. Bohnert, W.V. Kern, F. Verrey, M.G. Gruetter, K. Diederichs, K.M. Pos, Transport of drugs by the multidrug transporter AcrB involves an access and a deep binding pocket that are separated by a switch-loop, Proc. Natl. Acad. Sci. U. S. A. 109 (2012) 5687–5692.
[23] M.A. Seeger, K. Diederichs, T. Eicher, L. Brandstatter, A. Schiefner, F. Verrey, K.M. Pos, The AcrB efflux pump: conformational cycling and peristalsis lead to multidrug resistance, Curr. Drug Targets 9 (2008) 729–749.
[24] M.A. Seeger, C. Von Ballmoos, T. Eicher, L. Brandstätter, F. Verrey, K. Diederichs, K.M. Pos, Engineered disulfide bonds support the functional rotation mechanism of multidrug efflux pump AcrB, Nat. Struct. Mol. Biol. 15 (2008) 199–205.
[25] Y. Takatsuka, H. Nikaido, Covalently linked trimer of the AcrB multidrug efflux pump provides support for the functional rotating mechanism, J. Bacteriol. 191 (2009) 1729–1737.
[26] C. Oswald, H.-K. Tam, K.M. Pos, Transport of lipophilic carboxylates is mediated by transmembrane helix 2 in multidrug transporter AcrB, Nat. Commun. 7 (2016) 13819.
[27] S.A. Adcock, J.A. McCammon, Molecular dynamics: survey of methods for simulating the activity of proteins, Chem. Rev. 106 (2006) 1589–1615.
[28] M.Ø. Jensen, S. Park, E. Tajkhorshid, K. Schulten, Energetics of glycerol conduction through aquaglyceroporin GlpF, Proc. Natl. Acad. Sci. U. S. A. 99 (2002) 6731–6736.
[29] O.F. Lange, N.-A. Lakomek, C. Farès, G.F. Schröder, K.F.A. Walter, S. Becker, J. Meiler, H. Grubmüller, C. Griesinger, B.L. de Groot, Recognition dynamics up to

microseconds revealed from an RDC-derived ubiquitin ensemble in solution, Science 320 (2008) 1471–1475.
[30] J. Parkin, M. Chavent, S. Khalid, Molecular simulations of gram-negative bacterial membranes: a vignette of some recent successes, Biophys. J. 109 (2015) 461–468.
[31] J.P.G.L.M. Rodrigues, A.M.J.J. Bonvin, Integrative computational modeling of protein interactions, FEBS J. 281 (2014) 1988–2003.
[32] H.I. Ingólfsson, C.A. Lopez, J.J. Uusitalo, D.H. de Jong, S.M. Gopal, X. Periole, S.J. Marrink, The power of coarse graining in biomolecular simulations, Wiley Interdiscip. Rev. Comput. Mol. Sci. 4 (2014) 225–248.
[33] M. Karplus, R. Lavery, Significance of molecular dynamics simulations for life sciences, Isr. J. Chem. 54 (2014) 1042–1051.
[34] E. Lindahl, M.S.P. Sansom, Membrane proteins: molecular dynamics simulations, Curr. Opin. Struct. Biol. 18 (2008) 425–431.
[35] A. Ganesan, M.L. Coote, K. Barakat, Molecular dynamics-driven drug discovery: leaping forward with confidence, Drug Discov. Today 22 (2017) 249–269.
[36] M.A. Seeger, Membrane transporter research in times of countless structures, Biochim. Biophys. Acta Biomembr. (2017), http://dx.doi.org/10.1016/j.bbamem.2017.08.009.
[37] R. Schulz, A.V. Vargiu, F. Collu, U. Kleinekathöfer, P. Ruggerone, Functional rotation of the transporter AcrB: insights into drug extrusion from simulations, PLoS Comput. Biol. 6 (2010) e1000806.
[38] Z. Zuo, B. Wang, J. Weng, W. Wang, Stepwise substrate translocation mechanism revealed by free energy calculations of doxorubicin in the multidrug transporter AcrB, Sci. Rep. 5 (2015) 13905.
[39] Z. Zuo, J. Weng, W. Wang, Insights into the inhibitory mechanism of D13-9001 to the multidrug transporter AcrB through molecular dynamics simulations, J. Phys. Chem. B 120 (2016) 2145–2154.
[40] R. Schulz, A.V. Vargiu, P. Ruggerone, U. Kleinekathöfer, Role of water during the extrusion of substrates by the efflux transporter AcrB, J. Phys. Chem. B 115 (2011) 8278–8287.
[41] A.V. Vargiu, F. Collu, R. Schulz, K.M. Pos, M. Zacharias, U. Kleinekathöfer, P. Ruggerone, Effect of the F610A mutation on substrate extrusion in the AcrB transporter: explanation and rationale by molecular dynamics simulations, J. Am. Chem. Soc. 133 (2011) 10704–10707.
[42] X.-Q. Yao, H. Kenzaki, S. Murakami, S. Takada, Drug export and allosteric coupling in a multidrug transporter revealed by molecular simulations, Nat. Commun. 1 (2010) 117.
[43] X.-Q. Yao, N. Kimura, S. Murakami, S. Takada, Drug uptake pathways of multidrug transporter AcrB studied by molecular simulations and site-directed mutagenesis experiments, J. Am. Chem. Soc. 135 (2013) 7474–7485.
[44] Z. Wang, G. Fan, C.F. Hryc, J.N. Blaza, I.I. Serysheva, M.F. Schmid, W. Chiu, B.F. Luisi, D. Du, An allosteric transport mechanism for the AcrAB-TolC multidrug efflux pump, elife 6 (2017) e24905.
[45] G. Malloci, A. Vargiu, G. Serra, A. Bosin, P. Ruggerone, M. Ceccarelli, A database of force-field parameters, dynamics, and properties of antimicrobial compounds, Molecules 20 (2015) 13997–14021.
[46] J. Wang, R.M. Wolf, J.W. Caldwell, P.A. Kollman, D.A. Case, Development and testing of a general amber force field, J. Comput. Chem. 25 (2004) 1157–1174.
[47] D. Case, V. Babin, J. Berryman, R. Betz, Q. Cai, D. Cerutti, T. Cheatham III, T. Darden, R. Duke, H. Gohlke, A. Goetz, S. Gusarov, N. Homeyer, P. Janowski, J. Kaus, I. Kolossváry, A. Kovalenko, T. Lee, S. LeGrand, T. Luchko, R. Luo, B. Madej, K.M. Merz, F. Paesani, D.R. Roe, A.E. Roitberg, C. Sagui, R. Salomon-Ferrer, G. Seabra, C. Simmerling, W. Smith, J. Swails, R.C. Walker, J. Wang, R. Wolf, X. Wu, P. Kollman, Amber 14, University of California (CA), San Francisco, USA, 2014.
[48] M.J. Frisch, G.W. Trucks, H.B. Schlegel, G.E. Scuseria, M.A. Robb, J.R. Cheeseman, G. Scalmani, V. Barone, B. Mennucci, G.A. Petersson, H. Nakatsuji, M. Caricato, X. Li, H.P. Hratchian, A.F. Izmaylov, J. Bloino, G. Zheng, J.L. Sonnenberg, M. Hada, M. Ehara, K. Toyota, R. Fukuda, J. Hasegawa, M. Ishida, T. Nakajima, Y. Honda, O. Kitao, H. Nakai, T. Vreven, J.A.M. Jr, J.E. Peralta, F. Ogliaro, M. Bearpark, J.J. Heyd, E. Brothers, K.N. Kudin, V.N. Staroverov, R. Kobayashi, J. Normand, K. Raghavachari, A. Rendell, J.C. Burant, S.S. Iyengar, J. Tomasi, M. Cossi, N. Rega, J.M. Millam, M. Klene, J.E. Knox, J.B. Cross, V. Bakken, C. Adamo, J. Jaramillo, R. Gomperts, R.E. Stratmann, O. Yazyev, A.J. Austin, R. Cammi, C. Pomelli, J.W. Ochterski, R.L. Martin, K. Morokuma, V.G. Zakrzewski, G.A. Voth, P. Salvador, J.J. Dannenberg, S. Dapprich, A.D. Daniels, Ö. Farkas, J.B. Foresman, J.V. Ortiz, J. Cioslowski, D.J. Fox, Gaussian 09, Revision A.1, Gaussian, Inc., Wallingford CT, 2009.
[49] J.A. Maier, C. Martinez, K. Kasavajhala, L. Wickstrom, K.E. Hauser, C. Simmerling, ff14SB: improving the accuracy of protein side chain and backbone parameters from ff99SB, J. Chem. Theory Comput. 11 (2015) 3696–3713.
[50] W.L. Jorgensen, J. Chandrasekhar, J.D. Madura, R.W. Impey, M.L. Klein, Comparison of simple potential functions for simulating liquid water, J. Chem. Phys. 79 (1983) 926–935.
[51] I.S. Joung, T.E. Cheatham III, Determination of alkali and halide monovalent ion parameters for use in explicitly solvated biomolecular simulations, J. Phys. Chem. B 112 (2008) 9020–9041.
[52] J. Schlitter, M. Engels, P. Kruger, Targeted molecular dynamics: a new approach for searching pathways of conformational transitions, J. Mol. Graph. 12 (1994) 84–89.
[53] H. Grubmüller, B. Heymann, P. Tavan, Ligand binding: molecular mechanics calculation of the streptavidin-biotin rupture force, Science 271 (1996) 997–999.
[54] S. Izrailev, S. Stepaniants, M. Balsera, Y. Oono, K. Schulten, Molecular dynamics study of unbinding of the avidin-biotin complex, Biophys. J. 72 (1997) 1568–1581.
[55] G.M. Torrie, J.P. Valleau, Nonphysical sampling distributions in Monte Carlo free-energy estimation: umbrella sampling, J. Comput. Phys. 23 (1977) 187–199.
[56] B. Roux, The calculation of the potential of mean force using computer simulations, Comput. Phys. Commun. 91 (1995) 275–282.
[57] S. Kumar, J.M. Rosenberg, D. Bouzida, R.H. Swendsen, P.A. Kollman, The weighted histogram analysis method for free-energy calculations on biomolecules. I. The method, J. Comput. Chem. 13 (1992) 1011–1021.
[58] M.J. Abraham, D. van der Spoel, E. Lindahl, B. Hess, the GROMACS development team, GROMACS User Manual Version 5.1.4, (2016).
[59] W. Humphrey, A. Dalke, K. Schulten, VMD: Visual molecular dynamics, J. Mol. Graph. 14 (1996) 33–38.
[60] J.C. Phillips, R. Braun, W. Wang, J. Gumbart, E. Tajkhorshid, E. Villa, C. Chipot, R.D. Skeel, L. Kalé, K. Schulten, Scalable molecular dynamics with NAMD, J. Comput. Chem. 26 (2005) 1781–1802.
[61] H. Huang, E. Ozkirimli, C.B. Post, Comparison of three perturbation molecular dynamics methods for modeling conformational transitions, J. Chem. Theory Comput. 5 (2009) 1304–1314.
[62] F. Husain, H. Nikaido, Substrate path in the AcrB multidrug efflux pump of *Escherichia coli*, Mol. Microbiol. 78 (2010) 320–330.
[63] P.G. Kusalik, I.M. Svishchev, The spatial structure in liquid water, Science 265 (1994) 1219–1221.
[64] T. Imai, N. Miyashita, Y. Sugita, A. Kovalenko, F. Hirata, A. Kidera, Functionality mapping on internal surfaces of multidrug transporter AcrB based on molecular theory of solvation: implications for drug efflux pathway, J. Phys. Chem. B 115 (2011) 8288–8295.
[65] V.K. Ramaswamy, A.V. Vargiu, G. Malloci, J. Dreier, P. Ruggerone, Molecular rationale behind the differential substrate specificity of bacterial RND multi-drug transporters, Sci. Rep. 7 (2017) 8075.
[66] A.D. Kinana, A.V. Vargiu, H. Nikaido, Effect of site-directed mutations in multidrug efflux pump AcrB examined by quantitative efflux assays, Biochem. Biophys. Res. Commun. 480 (2016) 552–557.
[67] A. Verchère, M. Dezi, V. Adrien, I. Broutin, M. Picard, *In vitro* transport activity of the fully assembled MexAB-OprM efflux pump from *Pseudomonas aeruginosa*, Nat. Commun. 6 (2015) 6890.
[68] D. Du, Z. Wang, N.R. James, J.E. Voss, E. Klimont, T. Ohene-Agyei, H. Venter, W. Chiu, B.F. Luisi, Structure of the AcrAB-TolC multidrug efflux pump, Nature 509 (2014) 512–515.
[69] L.R. Forrest, R. Krämer, C. Ziegler, The structural basis of secondary active transport mechanisms, Biochim. Biophys. Acta Bioenerg. 1807 (2011) 167–188.
[70] K. Nagano, H. Nikaido, Kinetic behavior of the major multidrug efflux pump AcrB of *Escherichia coli*, Proc. Natl. Acad. Sci. U. S. A. 106 (2009) 5854–5858.
[71] S.P. Lim, H. Nikaido, Kinetic parameters of efflux of Penicillins by the multidrug efflux transporter AcrAB-TolC of *Escherichia coli*, Antimicrob. Agents Chemother. 54 (2010) 1800–1806.
[72] A.D. Kinana, A.V. Vargiu, H. Nikaido, Some ligands enhance the efflux of other ligands by the *Escherichia coli* multidrug pump AcrB, Biochemistry 52 (2013) 8342–8351.
[73] B. Wang, J. Weng, W. Wang, Free energy profiles of ion permeation and doxorubicin translocation in TolC, J. Theor. Comput. Chem. 13 (2014) 1450031.
[74] R. Mowla, Y. Wang, S. Ma, H. Venter, Kinetic analysis of the inhibition of the drug efflux protein AcrB using surface plasmon resonance, Biochim. Biophys. Acta Biomembr. (2017), http://dx.doi.org/10.1016/j.bbamem.2017.08.024.
[75] E.B. Tikhonova, Y. Yamada, H.I. Zgurskaya, Sequential mechanism of assembly of multidrug efflux pump AcrAB-TolC, Chem. Biol. 18 (2011) 454–463.
[76] A.D. Kinana, A.V. Vargiu, T. May, H. Nikaido, Aminoacyl β-naphthylamides as substrates and modulators of AcrB multidrug efflux pump, Proc. Natl. Acad. Sci. U. S. A. 113 (2016) 1405–1410.
[77] J. Vergalli, E. Dumont, B. Cinquin, L. Maigre, J. Pajovic, E. Bacqué, M. Mourez, M. Réfrégiers, J.-M. Pagès, Fluoroquinolone structure and translocation flux across bacterial membrane, Sci. Rep. 7 (2017) 9821.
[78] H. Sjuts, A.V. Vargiu, S.M. Kwasny, S.T. Nguyen, H.-S. Kim, X. Ding, A.R. Ornik, P. Ruggerone, T.L. Bowlin, H. Nikaido, K.M. Pos, T.J. Opperman, Molecular basis for inhibition of AcrB multidrug efflux pump by novel and powerful pyranopyridine derivatives, Proc. Natl. Acad. Sci. U. S. A. 113 (2016) 3509–3514.
[79] R. Nakashima, K. Sakurai, S. Yamasaki, K. Hayashi, C. Nagata, K. Hoshino, Y. Onodera, K. Nishino, A. Yamaguchi, Structural basis for the inhibition of bacterial multidrug exporters, Nature 500 (2013) 102–106.
[80] A.V. Vargiu, H. Nikaido, Multidrug binding properties of the AcrB efflux pump characterized by molecular dynamics simulations, Proc. Natl. Acad. Sci. U. S. A. 109 (2012) 20637–20642.
[81] E.C. Hobbs, X. Yin, B.J. Paul, J.L. Astarita, G. Storz, Conserved small protein associates with the multidrug efflux pump AcrB and differentially affects antibiotic resistance, Proc. Natl. Acad. Sci. U. S. A. 109 (2012) 16696–16701.
[82] K. Jin-Sik, J. Hyeongseop, S. Saemee, K. Hye-Yeon, L. Kangseok, H. Jaekyung, H, Nam-Chul, Structure of the tripartite multidrug efflux pump AcrAB-TolC suggests an alternative assembly mode, Mol. Cells 38 (2015) 180–186.